Journal of Power Sources 199 (2012) 341–345

Contents lists available at SciVerse ScienceDirect

Journal of Power Sources

journal homepage: www.elsevier.com/locate/jpowsour

Short communication

Three-dimensional core–shell Cu@Cu_6Sn_5 nanowires as the anode material for lithium ion batteries

Jizhang Chen [a], Li Yang [a,*], Shaohua Fang [a], Shin-ichi Hirano [b], Kazuhiro Tachibana [c]

[a] School of Chemistry and Chemical Engineering, Shanghai Jiaotong University, Shanghai 200240, China
[b] Hirano Institute for Materials Innovation, Shanghai Jiaotong University, Shanghai 200240, China
[c] Department of Chemistry and Chemical Engineering, Faculty of Engineering, Yamagata University, Yamagata 992-8510, Japan

ARTICLE INFO

Article history:
Received 7 May 2011
Received in revised form 9 August 2011
Accepted 12 October 2011
Available online 18 October 2011

Keywords:
Tin
Copper
Core–shell
Nanowire
Anode
Li-ion battery

ABSTRACT

Core–shell Cu@Cu_6Sn_5 nanowires with three-dimensional structure have been successfully synthesized via an electrodeposition process, using $Cu(OH)_2$ nanorods prepared by anodization as the substrate. Different temperatures have been employed to heat-treat Sn–Cu composites. After heat-treated at 80 °C, strong adherence of the active material Cu_6Sn_5 to the current collector is achieved, and the crystal structure becomes more stable, thus delivering best cycling performance of 0.162 mAh cm^{-2} after 200 cycles at 1 C. Furthermore, superior rate capability (as high as 20 C) is also obtained.

1. Introduction

The finite fossil fuel reserves and global warning linked to CO_2 emissions have promoted the developments of electric vehicles (BEV, HEV, and PHEV) [1]. As potential power sources for electric vehicles, lithium ion batteries with high energy density, high power density, and high safety are urgently required. Recently, alloy materials such as silicon (Si), tin (Sn), antimony (Sb), and germanium (Ge) have been investigated to offer high theoretical specific capacities, multiple times of carbon-based materials, and are expected to be promising anode materials for next-generation lithium ion batteries [2–7]. Among them, metallic tin delivers a theoretical specific capacity of 991 mAh g^{-1} or 7313 mAh cm^{-3} as $Li_{4.4}Sn$, much larger than 372 mAh g^{-1} or 833 mAh cm^{-3} of commercial graphite as LiC_6 [8,9]. In addition, tin has a higher operating potential than graphite and does not undergo solvent intercalation, consequently being less reactive and much safer than graphite [10]. Unfortunately, practical application of Sn is greatly restricted by its severe volume expansion–contraction (up to 360%) experienced in the course of lithium ion insertion–extraction electrochemical process. These volume changes would induce both mechanical failure and loss of electrical contact at the electrode, resulting in very rapid capacity fading. To solve this problem, three strategies have been proposed: (i) disperse Sn particles in a carbon matrix to buffer volume changes of Sn, since carbon is elastic and conductive [11–13]; (ii) decrease particle size of Sn to nanoscale, thus shortening diffusion length and accommodating large mechanical strain associated with structure and volume changes [14,15]; and (iii) introduce a second metal element to form active/inactive intermetallic compounds Sn–M (e.g., Cu_6Sn_5, $CoSn_3$, Ni_3Sn_4, $FeSn_2$), in which highly conductive framework are formed and severe pulverization can be lessened [16–21]. Despite the improvements of cycling and rate performances by these methods, it remains a significant challenge to develop effectual architecture to put Sn into practical application.

Recently, binder-free techniques such as electrodeposition, electroless plating, sputtering, and electron-beam deposition were reported to prepare Cu_6Sn_5/Sn anode materials on copper substrates [22–26]. Using foam-type substrates, several groups obtained Sn–Cu active materials with improved electrochemical performances [26–29]. Cu nanopillars were also reported as the substrate to electrodeposit Sn [30]. Although it showed better performances than Sn-covered Cu planar, most of Sn was in fact not well connected to Cu nanopillars, and the specific capacity was very low. Herein, we first report $Cu(OH)_2$ as the substrate to electrodeposit Cu_6Sn_5 anode material for lithium ion batteries, and core–shell Cu@Cu_6Sn_5 nanowires with three-dimensional structure were obtained. The morphology of nanowires favors Li^+ insertion–extraction process of alloy materials [5–7]. In addition,

* Corresponding author. Tel.: +86 21 54748917; fax: +86 21 54741297.
E-mail address: liyangce@sjtu.edu.cn (L. Yang).

0378-7753/$ – see front matter.
doi:10.1016/j.jpowsour.2011.10.043

our fabrication process (co-deposition) can provide great connection between the core (Cu) and the shell (Cu_6Sn_5). As-prepared Sn–Cu nanowires heat-treated at 80 °C delivered stable capacity of ca. 0.162 mAh cm^{-2} after 200 cycles at 1 C and superb rate performance (as high as 20 C).

2. Experimental

2.1. Sample preparation and characterization

$Cu(OH)_2$ nanorods substrate was prepared by galvanostatic anodization method, using a voltammetry tool HSV-100 (Hokuto Denko). Typically, a square copper foil (2 cm × 2 cm, 99.99%, Sinopharm Chemical Reagent Co., Ltd.) was pretreated in acetone and dilute hydrochloric acid, and then used as the working electrode (anode). A platinum wire of 5 cm in length was used as the counter electrode and kept 2.5 cm away from copper foil. The electrodes were immersed in 1 M NaOH aqueous solution, and 8 mA current was applied to perform the anodization process at room temperature. After 16 min, copper foil was taken out from NaOH solution and washed with deionized water thoroughly. Sn–Cu composite was prepared by electrodeposition, using anodized copper foil as the working electrode (cathode), and platinum wire as the counter electrode. The electrolyte was comprised of 3 g $K_2SnO_3 \cdot 3H_2O$, 3 g NaAc, and 1.5 g NaOH dissolved in 150 mL deionized water. −8 mA current was applied to perform the electrodeposition process at room temperature. After 60 min, copper foil was taken out from the electrolyte and washed with deionized water thoroughly, and subsequently dried under vacuum at room temperature. It was then heated at 80 °C for 24 h or calcined at 200 °C for 8 h under nitrogen. For comparison, $Cu(OH)_2$ particles obtained by anodizaion in 3 M NaOH aqueous solution were also used as the substrate to produce Su–Cu composite (denoted as Sn–Cu–P). The materials were characterized by X-ray diffraction measurement (XRD, Rigaku, D/max-Rbusing Cu Ka radiation), transmission electron microscopy (TEM, JEOL JEM-2010), and field emitting scanning electron microscopy (FE-SEM JEOL JSM-7401F).

2.2. Electrode preparation and electrochemical characterization

Electrochemical measurements were performed using coin-type half cells assembled in an argon-filled glove box (German, M. Braun Co., $[O_2] < 1$ ppm, $[H_2O] < 1$ ppm). For preparing the working electrode, as-prepared copper foil was cut in a rounded shape with the diameter of 14 mm. The electrodeposited Sn was measured to be ca. 0.61 mg for each electrode. Pure lithium foil was used as the counter electrode. A glass fiber (GF/A) from Whatman was used as the separator. The electrolyte consisted of a solution of 1 M $LiPF_6$ in ethylene carbonate and dimethyl carbonate (EC + DMC) (1:1 in volume), obtained from Zhangjiagang Guotai Huarong. Galvanostatic cycling of the assembled cells was carried out using a CT2001A cell test instrument (LAND Electronic Co.) under different current densities between cutoff voltages of 2 and 0.01 V at room temperature. Cyclic voltammetry (CV) and electrochemical impedance spectrum (EIS) were measured using a CHI660D electrochemical workstation.

3. Results and discussion

The synthesis procedure of core–shell Cu@Sn–Cu nanowires is described in Fig. 1. It can be seen that $Cu(OH)_2$ nanorods prepared by anodization were used as the substrate to perform electrodeposition. In the electrodeposotion process, $Cu(OH)_2$ was in situ reduced to Cu, Sn^{4+} was reduced to Sn, and Cu_6Sn_5 alloy was formed. This co-deposition process of Cu^{2+} and Sn^{4+} could provide much better connection of as-deposited Sn–Cu composite to the current collector Cu than directly electrodepositing Sn^{2+} or Sn^{4+} on Cu. As-deposited Sn–Cu composite was then heat-treated at different temperatures, i.e. room temperature (denoted as Sn–Cu-RT), 80 °C (Sn–Cu-80), and 200 °C (Sn–Cu-200).

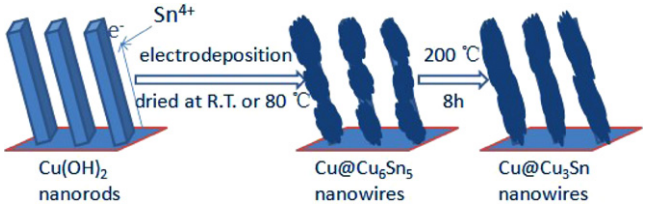

Fig. 1. Schematic illustration of the fabrication process.

Fig. 2 shows XRD patterns of our products. After anodization, orthorhombic $Cu(OH)_2$ (JCPDS 13-0420) was obtained. After electrodeposition, the XRD data of Sn–Cu-RT is in line with monoclinic Cu_6Sn_5 ($C2/c$), which did not change after heat treatment at 80 °C. This composite was then converted to orthorhombic Cu_3Sn (JCPDS 01-1240) for Sn–Cu-200.

The morphology and structure of our products have been investigated by SEM and TEM measurements. $Cu(OH)_2$ substrate is observed to be nanorods (Fig. 3a, b, and e) with the diameter of 100–200 nm. It is worth noting that $Cu(OH)_2$ nanorods are not perpendicular to copper foil, whereas interlacing with each other, possessing three-dimensional structure. In addition, the height of $Cu(OH)_2$ is about 6.58 μm, much higher than Cu nanopillars prepared by alumina oxide membrane [30]. Fig. 3c shows a panoramic SEM image of Sn–Cu-80, indicative of uniform structure. From Fig. 3d, we can see that the morphology of Sn–Cu-80 is nanowires. TEM image in Fig. 3f exhibits protuberant morphology, induced by electrodeposition of Cu_6Sn_5 on Cu. The inner part (core) is current collector copper, and the outer part (shell) is active material Cu_6Sn_5. HRTEM image gives a 0.295 nm lattice spacing, consistent with the lattice spacing of $(1\,1\,\bar{3})$ and $(2\,2\,\bar{1})$ planes of Cu_6Sn_5 (JCPDS 45-1488).

The electrochemical cycling performances of up to 200 cycles for four types of Sn–Cu composites were studied by the galvanostatic method at 1 C using 2016-type half cells (Fig. 4a). Clearly, the discharge capacity of Sn–Cu-200 dropped rapidly, with capacity retention of merely 17.6% at 2nd cycle. Such a poor capacity retention originates from the inactive nature of Cu_3Sn [31,32], and the degradation of electrolyte mainly contributed to the initial discharge capacity. As for Sn–Cu–P, it kept dropping down to merely 0.003 mAh cm^{-2} in 200th cycle, mainly caused by severe pulverization and disconnection of the active material. The cycling

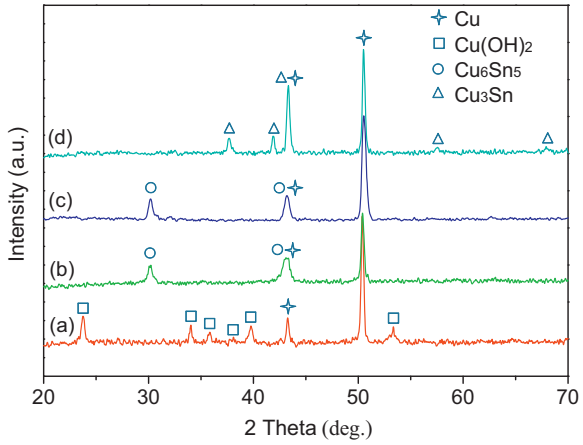

Fig. 2. XRD patterns of (a) Cu-based substrate and different Sn–Cu composites, (b) dried at R.T., (c) heated at 80 °C, and (d) calcined at 200 °C.

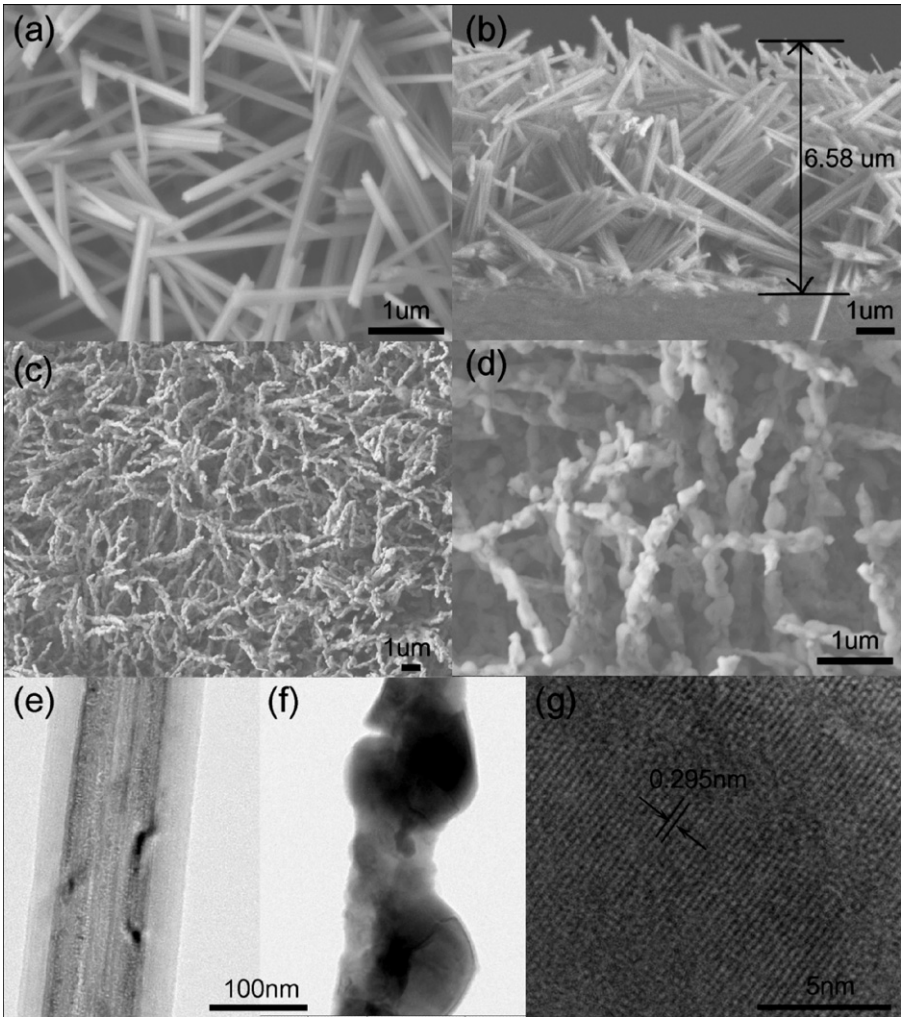

Fig. 3. SEM and TEM images of (a, b, and e) $Cu(OH)_2$ substrate and (c, d, f, and g) as-deposited Sn–Cu composite heated at 80 °C with different magnifications (b: cross-section micrograph).

performance of Sn–Cu-RT is obviously better than Sn–Cu–P, confirming that our configuration of three-dimensional nanowires favors electrochemical process. It is observed that Sn–Cu-80 gave the best cycling performance. We believe that heat treatment at 80 °C can provide more stable crystal structure and much stronger adherence of the active material Cu_6Sn_5 to the current collector Cu. The cycling behavior of Sn–Cu-80 can be divided into three regions, and this similar phenomenon has been explained in the previous report [33]. Differently, the discharge capacity of our product dropped down for initial five cycles, mainly caused by the severe degradation of electrolyte to form SEI film, which is especially significant for our product since as-deposited composite possesses a very large specific surface area. In the second region of 6th to 35th cycles, the isolated electrode material gradually connected to the main part and recovered activity again, thus leading to slight capacity rise. Then in the third region, repeated volume expansion and contraction would cause part of the active material crack and disconnect to the current collector, decreasing the capacity. After appropriate amount of Sn was detached, the volume changes can be effectively buffered, so the cycling became stable and 0.162 mAh cm^{-2} was finally obtained in 200th cycle, 8 times of Sn-covered Cu nanopillars [30]. The discharge/charge curves of Sn–Cu-80 shown in Fig. 4b present coulumbic efficiencies of 85.2%, 93.5%, and 94.7% in initial three cycles, respectively. The sloping potential plateau below 0.3 V is characteristic of the transformations of Cu_6Sn_5 into Li_2CuSn and subsequently Li_2CuSn into $Li_{4.4}Sn$ [34,35]. The nearly overlapped curves of 2nd and 3rd cycles suggest superb reversible electrochemical behavior.

Fig. 5 reveals XRD patterns of different Sn–Cu composites after 200 cycles. The characteristic peaks of Cu_6Sn_5 disappeared for Sn–Cu-RT, and high-temperature solid solutions $Cu_{41}Sn_{11}$ and $Cu_{10}Sn_3$ formed, which are also active to lithium ion [36]. The crystal structure did not change for Sn–Cu-80 after cycles, whereas the characteristic peaks turned to be weak, indicating that part of Sn became amorphous after electrochemical process, similar to Si and Ge [6,7]. In the case of Sn–Cu-200, no phase change occurred, confirming its inactive nature.

The cyclic voltammograms of Sn–Cu-80 conducted at a scan rate of 0.5 mV s^{-1} are shown in Fig. 6a. Two tiny cathodic peak at 0.61 V and 0.65 V originating from trace pure Sn alloying with lithium can be observed in 1st cycle, and they became very weak in 2nd and 3rd cycles. The second cathodic peak below 0.3 V can be assigned to the formation of $Li_{4.4}Sn$ from Cu_6Sn_5, according well with above discharge curves. In the anodic curve, two peaks at 0.73 and 0.92 V are visible, which shifted to 0.71 and 0.85 V in 2nd cycle, 0.67 and 0.84 V in 3rd cycle, and they are ascribed to the de-alloying process. Electrochemical impedance spectroscopy measurements were carried out at the open circuit potential in the frequency range from 1×10^5 Hz to 1 Hz with perturbation amplitude of 5 mV and typical Nyquist plots are given in Fig. 6b. The high frequency intercept

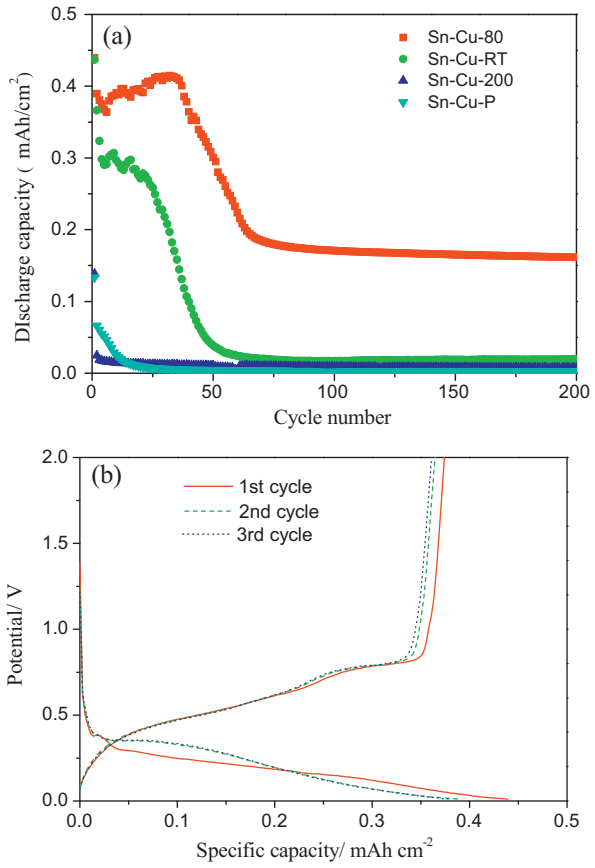

Fig. 4. (a) Cycling performances of different Sn–Cu composites at 1 C; (b) initial three discharge/charge curves of Cu@Cu_6Sn_5 nanowires heated at 80 °C.

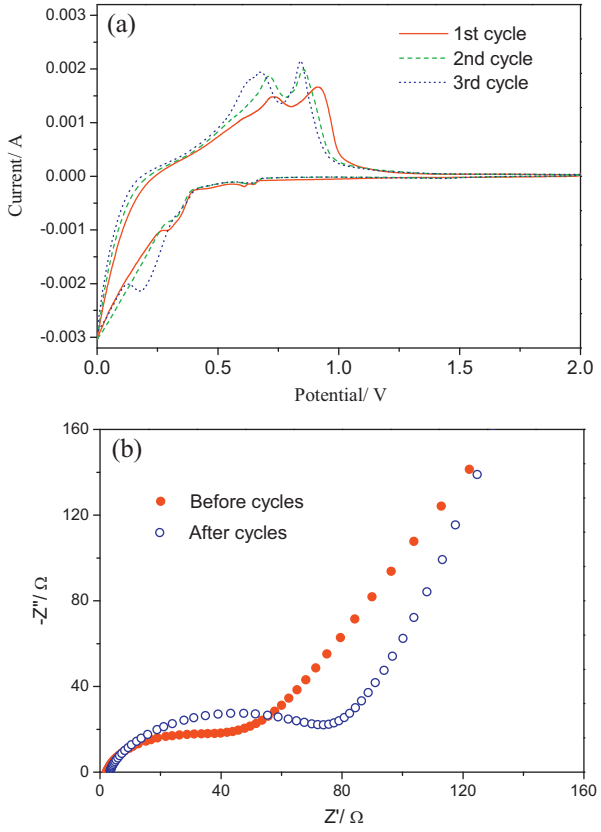

Fig. 6. (a) CV curves of Cu@Cu_6Sn_5 nanowires heated at 80 °C and (b) Nyquist plots before and after 200 galvanostatic cycles.

of the semicircle is generally considered as the bulk resistance of electrodes, electrolyte, and separator, which experienced little variation after 200 cycles. The depressed semicircles at high/medium frequency are reflective of SEI layer and charge transfer impedance, and the inclined line at low frequency corresponds to lithium diffusion within the active material. After 200 cycles, the impedance only increased a little amount, suggesting that pulverization can be effectively suppressed for our product.

Sn–Cu-80 was further discharged at progressing higher rates after 200 cycles, as shown in Fig. 7. The reversible capacities are 0.160 mAh cm^{-2} at 1 C, 0.139 mAh cm^{-2} at 2 C, 0.102 mAh cm^{-2} at 5 C, 0.073 mAh cm^{-2} at 10 C, 0.053 mAh cm^{-2} at 20 C, and finally back to 0.153 mAh cm^{-2} at 1 C again, manifesting that as-prepared Sn–Cu composite can sustain high current density without structural collapse.

From Fig. 8, we can observe SEM and TEM images of Sn–Cu-80 after electrochemical process. After 3 galvanostatic cycles, nanowires became thicker and rougher. After 200 cycles, this composite became much rougher, and even some small particles were visible on the surface, caused by the inevitable little pulverization of Sn, which is also the origin of capacity loss in initial cycles. It is noted that the morphology of nanowires and three-dimensional

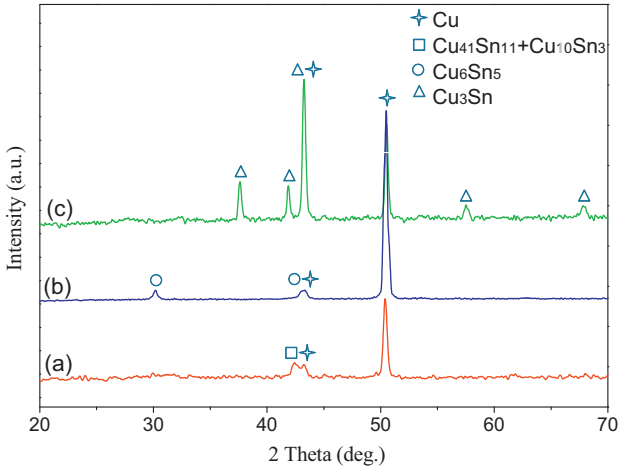

Fig. 5. XRD patterns of different Sn–Cu composites (a) dried at R.T., (b) heated at 80 °C, and (c) calcined at 200 °C, after 200 galvanostatic cycles.

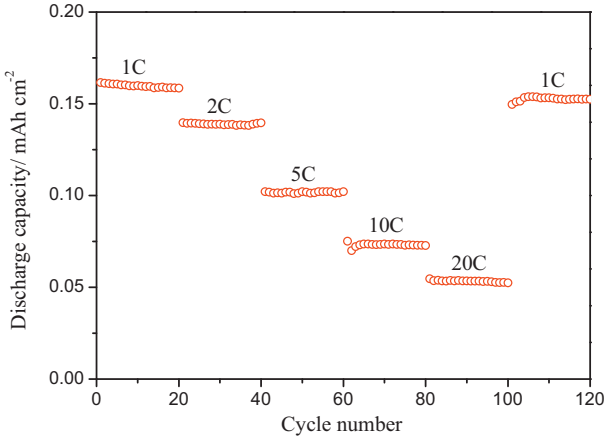

Fig. 7. Rate performance of Cu@Cu_6Sn_5 nanowires heated at 80 °C after 200 cycles from 1 C to 20 C for 20 cycles at each rate.

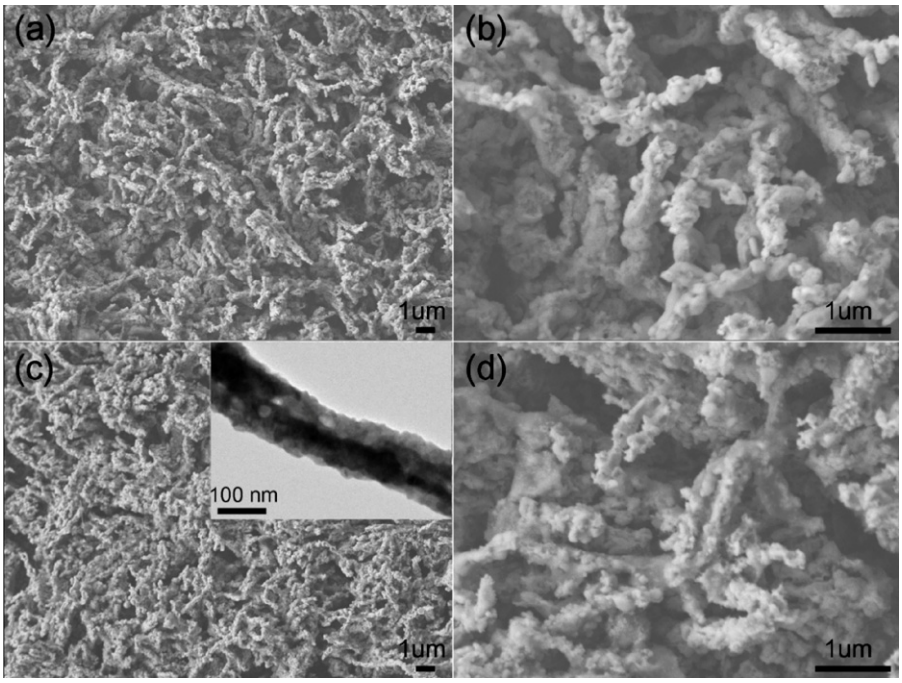

Fig. 8. SEM images of $Cu@Cu_6Sn_5$ nanowires heated at 80 °C (a and b) after 3 cycles and (c and d) after 200 cycles. The inset shows TEM image after 200 cycles.

structure were maintained, contributing to stable cycling performance after initial cycles. Consequently, we believe that the superb rate and cycling performances are rooted in its peculiar structure: (i) co-deposition strengthens the bonding force between the active material (shell) and the current collector (core), and the contact area is extremely large; (ii) nanowires have facile strain relaxation, and the small size of the active material on nanowires can alleviate pulverization and aggregation, and facilitate the diffusion of both Li^+ and e^-; (iii) three-dimensional architecture provides huge contact area between the electrode and the electrolyte and enough void space to buffer volumes changes during the electrochemical process.

4. Conclusions

In this article, $Cu(OH)_2$ nanorods prepared by anodization were used as the substrate to produce three-dimensional core–shell $Cu@Cu_6Sn_5$ nanowires by electrodeposition. $Cu@Cu_6Sn_5$ nanowires heat treated at 80 °C showed interesting capacity evolution and final stable capacity of 0.162 mAh cm^{-2} after 200 cycles at 1 C. Superior rate performance conducted after 200 galvanostatic cycles was also obtained. This improved electrochemical behavior could be assigned to the core–shell nanowires morphology and three-dimensional structure, which are maintained after galvanostatic cycles.

Acknowledgements

This work was performed with the financial support from the National Natural Science Foundation of China (Grants No. 21103108 and 21173148), Toyota Motor Corporation, and Shanghai Jiao Tong University Innovation Fund For Postgraduates. The authors thank the Research Center of Analysis and Measurement of Shanghai Jiao-Tong University for the help of TEM characterization.

References

[1] B. Scrosati, J. Garche, J. Power Sources 195 (2010) 2419.
[2] H. Kim, B. Han, J. Choo, J. Cho, Angew. Chem. Int. Ed. 47 (2008) 10151.
[3] G. Derrien, J. Hassoun, S. Panero, B. Scrosati, Adv. Mater. 19 (2007) 2336.
[4] Y. Wang, J.Y. Lee, Angew. Chem. Int. Ed. 45 (2006) 7039.
[5] C.K. Chan, X.F. Zhang, Y. Cui, Nano Lett. 8 (2008) 307.
[6] C.K. Chan, H.L. Peng, G. Liu, K. Mcllwrath, X.F. Zhang, R.A. Huggins, Y. Cui, Nat. Nano 3 (2008) 31.
[7] L.F. Cui, R. Ruffo, C.K. Chan, H.L. Peng, Y. Cui, Nano Lett. 9 (2009) 491.
[8] M. Winter, J.O. Besenhard, Electrochim. Acta 45 (1999) 31.
[9] I.A. Courtney, J.R. Dahn, J. Electrochem. Soc. 144 (1997) 2045.
[10] M. Winter, J.O. Besenhard, M.E. Spahr, P. Novák, Adv. Mater. 10 (1998) 725.
[11] W.M. Zhang, J.S. Hu, Y.G. Guo, S.F. Zheng, L.S. Zhong, W.G. Song, L.J. Wan, Adv. Mater. 20 (2008) 1160.
[12] Y. Yu, L. Gu, C.L. Wang, A. Dhanabalan, P.A. van Aken, J. Maier, Angew. Chem. Int. Ed. 48 (2009) 6485.
[13] G.X. Wang, B. Wang, X.L. Wang, J. Park, S.X. Dou, H. Ahn, K. Kim, J. Mater. Chem. 19 (2009) 8378.
[14] Y.H. Yu, Q. Yang, D.H. Teng, X.P. Yang, S. Ryu, Electrochem. Commun. 12 (2010) 1187.
[15] G.L. Cui, Y.S. Hu, L.J. Zhi, D.Q. Wu, I. Lieberwirth, J. Maier, K. Müllen, Small 3 (2007) 2066.
[16] W.J. Cui, F. Wang, J. Wang, H.J. Liu, C.X. Wang, Y.Y. Xia, J. Power Sources 196 (2011) 3633.
[17] X.L. Wang, W.Q. Han, J.J. Chen, J. Graetz, ACS Appl. Mater. Interfaces 2 (2010) 1548.
[18] M.G. Kim, S. Sim, J. Cho, Adv. Mater. 22 (2010) 5154.
[19] J. Hassoun, S. Panero, P. Simon, P.L. Taberna, B. Scrosati, Adv. Mater. 19 (2007) 1632.
[20] X.Y. Fan, F.S. Ke, G.Z. Wei, L. Huang, S.G. Sun, J. Alloys Compd. 476 (2009) 70.
[21] S.H. Ju, H.C. Jang, Y.C. Kang, J. Power Sources 189 (2009) 163.
[22] R.H. Kim, D.H. Nam, H.S. Kwon, J. Power Sources 195 (2010) 5067.
[23] J.W. Park, J.Y. Eom, H.S. Kwon, Electrochim. Acta 55 (2010) 1825.
[24] Y.S. Lin, J.G. Duh, H.S. Sheu, J. Alloys Compd. 509 (2011) 123.
[25] R.Z. Hu, M.Q. Zeng, M. Zhu, Electrochim. Acta 54 (2009) 2843.
[26] L.G. Xue, Z.H. Fu, Y. Yao, T. Huang, A.S. Yu, Electrochim. Acta 55 (2010) 7310.
[27] Z.J. Du, S.C. Zhang, T. Jiang, Z.M. Bai, Electrochim. Acta 55 (2010) 3537.
[28] Q.Y. Li, S.J. Hua, H.Q. Wang, F.P. Wang, X.X. Zhong, X.Y. Wang, Electrochim. Acta 54 (2009) 5884.
[29] M. Yao, K. Okuno, T. Iwaki, T. Awazu, T. Sakai, J. Power Sources 195 (2010) 2077.
[30] L. Bazin, S. Mitra, P.L. Taberna, P. Poizot, M. Gressier, M.J. Menu, A. Barnabé, P. Simon, J.M. Tarascon, J. Power Sources 188 (2009) 578.
[31] Tamura, R. Ohshita, M. Fujimoto, M. Kamino, S. Fujitani, J. Electrochem. Soc. 150 (2003) A679.
[32] J.Y. Kwon, J.H. Ryu, Y.S. Jung, S.M. Oh, J. Alloys Compd. 509 (2011) 7595.
[33] H.C. Shin, M. Liu, Adv. Funct. Mater. 4 (2005) 582.
[34] D. Larcher, L.Y. Beaulieu, D.D. MacNeil, J.R. Dahn, J. Electrochem. Soc. 147 (2000) 1658.
[35] L. Fransson, E. Nordström, K. Edström, L. Häggström, M.M. Thackeray, J. Electrochem. Soc. 149 (2002) A736.
[36] A. Finke, P. Poizot, C. Guéry, J.M. Tarascon, J. Electrochem. Soc. 152 (2005) A2364.